JACS
JOURNAL OF THE AMERICAN CHEMICAL SOCIETY

ARTICLE

pubs.acs.org/JACS

Molecular-Level Examination of Cu^{2+} Binding Structure for Amyloid Fibrils of 40-Residue Alzheimer's β by Solid-State NMR Spectroscopy

Sudhakar Parthasarathy,[†] Fei Long,[†] Yifat Miller,[‡] Yiling Xiao,[†] Dan McElheny,[†] Kent Thurber,[⊥] Buyong Ma,[§] Ruth Nussinov,[§,∥] and Yoshitaka Ishii*[,†]

[†]Department of Chemistry, University of Illinois at Chicago, Chicago, Illinois 60607, United States

[‡]Center for Cancer Research Nanobiology Program, NCI-Frederick, Frederick, Maryland 21702, United States

[§]Basic Research Program, SAIC-Frederick, Inc. Center for Cancer Research Nanobiology Program NCI-Frederick, Frederick, MD 21702, United States

[⊥]Laboratory of Chemical Physics, NIDDK, National Institutes of Health, Bethesda Maryland 20892, United States

[∥]Sackler Institute of Molecular Medicine, Department of Human Genetics and Molecular Medicine, Sackler School of Medicine, Tel Aviv University, Tel Aviv 69978, Israel

Supporting Information

ABSTRACT: Cu^{2+} binding to Alzheimer's β (Aβ) peptides in amyloid fibrils has attracted broad attention, as it was shown that Cu ion concentration elevates in Alzheimer's senile plaque and such association of Aβ with Cu^{2+} triggers the production of neurotoxic reactive oxygen species (ROS) such as H_2O_2. However, detailed binding sites and binding structures of Cu^{2+} to Aβ are still largely unknown for Aβ fibrils or other aggregates of Aβ. In this work, we examined molecular details of Cu^{2+} binding to amyloid fibrils by detecting paramagnetic signal quenching in 1D and 2D high-resolution ^{13}C solid-state NMR (SSNMR) for full-length 40-residue Aβ(1−40). Selective quenching observed in ^{13}C SSNMR of Cu^{2+}-bound Aβ(1−40) suggested that primary Cu^{2+} binding sites in Aβ(1−40) fibrils include N_ε in His-13 and His-14 and carboxyl groups in Val-40 as well as in Glu sidechains (Glu-3, Glu-11, and/or Glu-22). ^{13}C chemical shift analysis demonstrated no major structural changes upon Cu^{2+} binding in the hydrophobic core regions (residues 18−25 and 30−36). Although the ROS production via oxidization of Met-35 in the presence of Cu^{2+} has been long suspected, our SSNMR analysis of $^{13}C_\varepsilon H_3-S-$ in M35 showed little changes after Cu^{2+} binding, excluding the possibility of Met-35 oxidization by Cu^{2+} alone. Preliminary molecular dynamics (MD) simulations on $Cu^{2+}-A\beta$ complex in amyloid fibrils confirmed binding sites suggested by the SSNMR results and the stabilities of such bindings. The MD simulations also indicate the coexistence of a variety of Cu^{2+}-binding modes unique in Aβ fibril, which are realized by both intra- and intermolecular contacts and highly concentrated coordination sites due to the in-register parallel β-sheet arrangements.

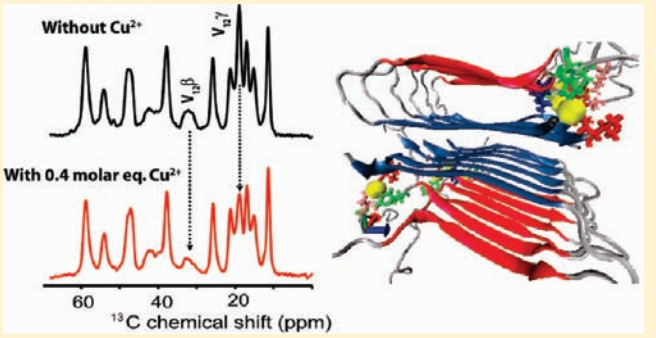

INTRODUCTION

Alzheimer's disease (AD) is characterized by the deposition of senile plaques and neural degeneration. Alzheimer's amyloid β (Aβ) peptides are a primary component of the senile plaques.[1,2] Among Aβ peptides ranging from 39 to 43 residues, 40-residue Aβ(1−40) and 42-residue Aβ(1−42) are the two major species found in plaque.[2] In AD, the metal ion homeostasis appears to be severely damaged, resulting in increased concentrations of Cu and Zn ions in senile plaque, which reach 400 μM and 1 mM, respectively[3] or ∼10-fold compared with the region outside the plaque.[4,5] More interestingly, it was shown that in association with Cu^{2+}, Aβ produces reactive oxygen species (ROS) such as H_2O_2 in vitro,[6] reportedly through the reduction of Cu^{2+} to Cu^{+} in association with M35[7] and/or biochemical reductants such as ascorbate.[8] The toxicity of Aβ can be greatly attenuated by H_2O_2 scavengers[9] and metal chelator in vitro.[6,10] Indeed, Aβ fibrils strongly bind Cu^{2+} ions.[11−13] Although the mechanisms of neural cell deaths and oxidative stress in AD are still debated, these events may be explained by the ROS generated on the redox-active Cu^{2+} ions bound on Aβ fibrils, which was observed in vitro. Small molecules which target metal−Aβ interactions have been tested as potential therapeutic agents,[14−16] including one in a clinical trial.[14] Thus, intensive efforts have been made to understand the molecular details of Cu^{2+}-binding to Aβ.[8,17−33] On the other hand, most structural studies on $Cu^{2+}-A\beta$ binding were performed on soluble model peptides[19−24,29] or monomeric Aβ;[25−27,33] however, some of these reports are controversial.

Solution NMR studies by Hou and Zagorski on monomeric Aβ(1−40) indicated specific binding of Cu^{2+} to sidechains of

Received: August 11, 2010
Published: February 22, 2011

   dx.doi.org/10.1021/ja1072178 | J. Am. Chem. Soc. 2011, 133, 3390–3400

H6, H13, and H14 by their upfield ^{1}H shifts, while suggesting the lack of association of D1 and Y10 with Cu^{2+} through little perturbation on their ^{1}H sidechain shifts.[27] The Cu^{2+} binding to the N-terminal region is consistent with a recent NMR study indicating paramagnetic relaxation enhancement on the residue 3-16 upon the addition of Cu^{2+} to monomeric Aβ(1−40).[25] EPR spectra of Cu^{2+}-bound Aβ(1−16), Aβ(1−28), and Aβ(1−42) monomers show quite similar spectral features for Cu^{2+};[19−21] it has been proposed that these EPR spectra suggests the presence of two types of Cu^{2+} binding sites, both of which are likely to have 4-coordination geometries such as 2N/2O and 3N/1O coordination to Cu^{2+}.[19−21] This is consistent with the solution NMR results[27] since two nitrogens of His imidazole rings typically offer coordination to Cu^{2+}.[34] More detailed isotope-edited EPR studies on Aβ(1−16) suggested Cu^{2+} coordination to D1, H6, H13 (or H14) for one spectral component (component I; $A_{//} = 162 \pm 3$ G and $g_{//} = 2.272$) and the second Cu^{2+} coordination to A2, H6, H13, H14 for the other minor spectral component at a neutral pH (component II; $A_{//} = 148 \pm 3$ G and $g_{//} = 2.227$).[19,20] In contrast, a recent EPR study on monomeric Aβ(1−28) suggested octahedral coordination by D1, D7, H6, H13, H14 for an EPR spectrum having similar yet distinguishable EPR parameters (component I: $A_{//} = 170$ G and $g_{//} = 2.27$; component II: $A_{//} = 156$ G and $g_{//} = 2.22$).[21] Although these Aβ monomer and fragments may have different metal binding modes, a conclusive structural model of Cu^{2+}−Aβ complex has not been established even for the soluble model systems (see Table 1 in ref 8 for example). More importantly, monomeric Aβ is nontoxic; a question relevant to the mechanism of AD is, therefore, Cu^{2+} binding structure in Aβ aggregates. Recent EPR studies on Cu^{2+}-bound amyloid fibril of Aβ(1−40) and Aβ(1−42) report the presence of, at least, two types of binding sites that also have 4-coordination geometries.[21,28,31,35] However, beyond the similarity of the EPR spectra of the Aβ fibrils with those of more well studied soluble Aβ fragments, scarce site specific information on metal binding modes has been obtained for Aβ fibrils. A recent EPR study on Aβ(1−28) showed no notable changes in the EPR by H6A or H14A mutation.[21] Thus, similarity in conventional continuous wave (cw) EPR spectra among Cu^{2+}-bound Aβ with varied sequences may not be sufficient to deduce Cu^{2+} coordination structure uniquely. Rather, coordination to Cu^{2+} involving different His residues and other ligands can yield very similar 1D EPR spectra as long as the local environments around Cu^{2+} are similar. On Cu^{2+} binding to oligomeric Aβ, there were some interesting studies,[25,35] yet the nature of these oligomeric species has not been well-defined. A recent study by solid-state NMR (SSNMR), a powerful method for structural analysis of protein aggregates[36−46] and other proteins,[47−62] indicated Cu^{2+} binding to Aβ in membrane environments.[63] Despite the broad attention and the intense efforts presented in the previous studies,[8,17−25,27−29] the exact Cu^{2+} binding sites of Aβ fibrils *have not been identified with any site-specificity*. Lack of site-specific structural information has also severely limited our molecular-level understanding on structural changes of Aβ fibrils upon Cu^{2+} binding. Such detailed structural information would be highly valuable for revealing still unknown mechanisms of the toxicity for Aβ aggregates and designing metal binding inhibitors for amyloid aggregates.[14−16]

Here, we present the first systematic study to address molecular details of Cu^{2+} binding on amyloid fibrils of full-length Aβ(1−40) by SSNMR. With the recent advance in SSNMR for paramagnetic proteins,[45,47,64−67] we examine the possibility of identifying site-specific Cu^{2+} binding to Aβ(1−40) fibrils and molecular-level structural changes upon the binding. Our SSNMR data show a lack of perturbation to ^{13}C chemical shifts by Cu^{2+} binding and suggest that the parallel β-sheet structures in the hydrophobic core regions of Aβ(1−40) fibrils are not reorganized into different structures by Cu^{2+} binding for the first time. Molecular dynamics (MD) simulations that take account of the amyloid fibril structure suggest that Cu^{2+} binding to Aβ in fibril is likely to involve the novel binding modes that are not possible in soluble fragments or monomers of Aβ.

RESULTS AND DISCUSSION

First, we examined the morphological changes of amyloid fibril after Cu^{2+} binding. Although it has been proposed that Cu^{2+} or Zn^{2+} binding to Aβ monomers may modulate misfolding kinetics,[27,30,35,68,69] in this work, we focus on structural changes due to Cu^{2+} binding after the fibril formation. Figure 1a and b shows transmission electron microscopy (TEM) images of Aβ fibrils without and with 0.4 mol equiv $CuCl_2$, respectively. The fibrils without Cu^{2+} have a diameter of ∼9 nm and a length of >1 μm, which are consistent with previous reports.[70] The morphology of the Aβ fibrils is retained after Cu^{2+} was bound to fibrils. Although it is difficult to deduce any molecular-level structural changes from the data, it is likely that Cu^{2+} binding does not substantially destabilize the amyloid fibril structure. Binding of Cu^{2+} to Aβ fibrils was determined by photometric assay using *N,N,N′,N′*-tetraethylthiuram disulfide as a Cu^{2+} indicator.[71] We confirmed that more than 95% of Cu^{2+} was bound to Aβ(1−40) for both $CuCl_2$ and CuGly when the ratio of Cu^{2+} to Aβ ($f_{Cu/A\beta}$) was 0.5 or less (see the Supporting Information (SI)). However, at $f_{Cu/A\beta} = 1.0$, 5.3% and 15% of Cu^{2+} ions were *not* bound to Aβ fibrils for $CuCl_2$ and CuGly, respectively (see the SI). On the basis of these results, we selected $f_{Cu/A\beta} = 0.4$ throughout the following SSNMR study as a condition where nearly all Cu^{2+} ions are *strongly* bound to Aβ fibrils.

Next, we examined whether any site-specific binding of Cu^{2+} can be detected by SSNMR for Aβ(1−40) fibrils. Figure 1c show a comparison of the aliphatic region of 1D ^{13}C CPMAS SSNMR spectra of Aβ(1−40) amyloid fibrils (black) without and (red) with 0.4 mol equiv of Cu^{2+} to Aβ. The Aβ(1−40) samples were isotope-labeled with uniformly ^{13}C- and ^{15}N-labeled amino acids at V12, F20, A21, I31, G33, and $^{13}C_\varepsilon$-selectively labeled M35 (see the SI). Interestingly, most sites display no significant changes in the signal intensities. This includes $^{13}C_\varepsilon$ of M35 (green arrow), which has been long suspected as the site that is responsible for the production of H_2O_2 through interactions with Cu^{2+}.[72,73] If the M35 sidechain (−S−$C_\varepsilon H_3$) is oxidized into −SO−CH_3 as hypothesized previously,[7] $^{13}C_\varepsilon$ shift at 15.6 ppm should be altered to ∼40 ppm.[74] However, no major changes in the signal intensity or chemical shift were observed for $^{13}C_\varepsilon$ M35 after a month. In contrast, signal intensities drop by 36% and 27% selectively for $^{13}C_\gamma$ and $^{13}C_\beta$ of V12 (orange arrows), respectively, upon Cu^{2+} binding. The site is nearby to H13/H14, which were reported to interact with Cu^{2+} for Aβ(1−40) monomer.[27] These results suggest that the effect of Cu^{2+} binding to fibrils is site specific, quenching the signals for sites in the vicinity of Cu^{2+} (V12 in this case). In a recent SSNMR study of Cu, Zn SOD, signal quenching of ^{13}C within a ∼5 Å radius of Cu^{2+} was reported.[47] Here, we utilize such paramagnetic quenching to identify Cu^{2+} binding sites in the aggregated form of the Aβ proteins.

Figure 1d shows a comparison of 2D ^{13}C/^{13}C spectra of the same Aβ fibril samples (black) without and (red) with Cu^{2+} bound to Aβ in a superposition. Most of the signals are well-resolved without signal overlap. Remarkably, the Cu^{2+}-bound fibril have nearly identical chemical shift positions (within ±0.2 ppm) and intensities with those for the Cu^{2+}-free fibril, except

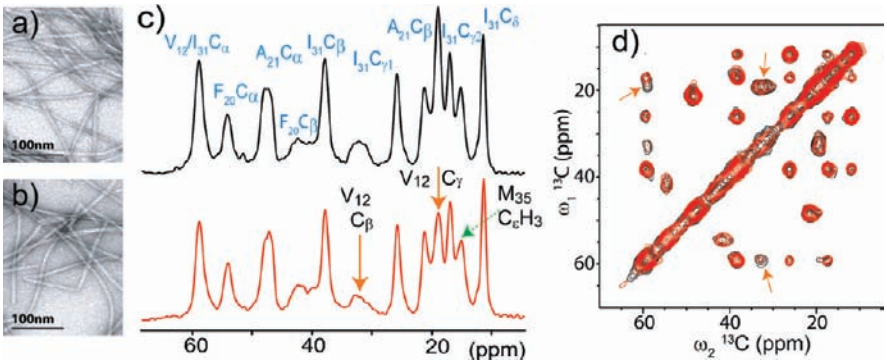

Figure 1. Transmission electron microscopy images of Aβ(1−40) fibrils (a) without and (b) with Cu^{2+}, which is 0.4 mol equiv to Aβ. Cu^{2+} ions were added after the fibril formation was complete throughout this work. (c) Comparison of 1D ^{13}C cross-polarization magic-angle spinning (CPMAS) spectra of Aβ(1−40) fibrils without (black) and with (red) 0.4 mol equiv of Cu^{2+}, together with signal assignments. The samples were labeled with uniformly ^{13}C-, ^{15}N-labeled amino acids at V12, F20, A21, I31, G33 and with $^{13}C_\varepsilon H_3$ selectively labeled at M35. (d) Comparison of the 2D ^{13}C/^{13}C correlation spectra for the same fibrils samples without (black) and with (red) Cu^{2+}. The spectra were obtained at MAS at 20 kHz. In (d) an fpRFDR sequence of 1.6 ms[87] was used for ^{13}C/^{13}C exchange.

for the V12 signals (orange arrows). Since ^{13}C chemical shifts are a probe very sensitive to protein conformations, this presents interesting evidence that the site-specific Cu^{2+} binding does not alter the conformations of Aβ in the β-sheet cores, including F20, A21, I31. Additional results below support this finding. Thus, we concluded that Cu^{2+}-binding does not introduce major conformation changes except for the N- and C-terminal regions, where binding is likely to take place, as will be discussed.

On the basis of the above results, we hypothesized that Cu^{2+} ions are interacting with H13 and H14 side chains in the Aβ fibril, and with other neighboring residues. To test this, we performed ^{13}C SSNMR of Aβ(1−40) fibril samples in which one of these residues was uniformly ^{13}C-labeled. Figure 2a and b show a 1D ^{13}C CPMAS spectra of (a) H13 and (b) H14 sidechains for Aβ fibrils (black) without and (red) with Cu^{2+} bound to Aβ, together with signal assignments. Clearly, the signals for both H13 and H14 are quenched considerably by Cu^{2+}. Spectral analysis of the aromatic sidechains shows that signals for $^{13}C_\delta$ and $^{13}C_\varepsilon$ in H13/H14 are quenched by 30−60%, while those for C_γ are quenched less (by ∼15%). This suggests that the Cu^{2+} ion favors coordination to N_ε in H13 and H14, which is one bond away from $^{13}C_\delta$ and $^{13}C_\varepsilon$, over that to N_δ. As a control, we examined paramagnetic quenching for F20 (Figure 2c), which shows nearly no quenching. Previous studies indicated the involvement of the N_δ/N_ε of histidine in Aβ(1−40) in Cu^{2+} binding.[26,27,75] Raman spectroscopic studies[26] shows that Aβ(1−40) precipitates obtained by the addition of Cu^{2+} to a Aβ solution display Cu^{2+} coordination to N_ε in His, while Aβ(1−40) monomers in a solution show Cu^{2+} coordination to N_δ at pH 7.4. Barnham et al.[75] reported that Aβ(1−40) having *N*-methylated His for N_ε at position His-6, -13, and -14 has weaker metal−ligand interaction than WT Aβ or Aβ(1−40) having *N*-methylated His for N_δ. The results are consistent with our finding. To the best of our knowledge, this is the first experimental data that directly demonstrate the association of Cu^{2+} with H13 and H14 of Aβ(1−40) in amyloid fibrils with site resolution.

Figure 2d shows the summary of the residues quenched by Cu^{2+} binding for six Aβ samples selectively isotope-labeled at different sites (see the SI). Only a limited number of aliphatic side chains were quenched by Cu^{2+} bound to Aβ (see Figure S2 in the SI). Apart from the significant changes in the N-terminal region, V24, and V39, other sites in the residues 17−38 show very limited

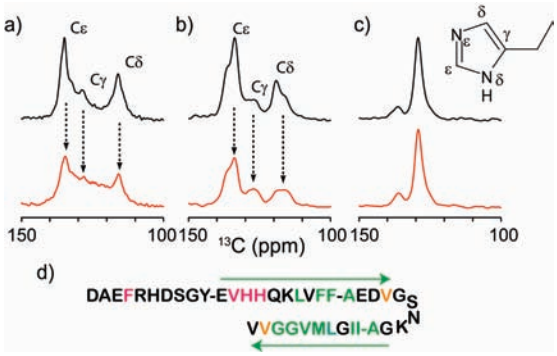

Figure 2. Aromatic regions of ^{13}C CPMAS spectra for (a) H13, (b) H14, and (c) F20 sidechains for Aβ(1−40) fibrils in the hydrated state (black) without and (red) with Cu^{2+}. (d) Amino acid sequence of Aβ(1−40) and the extent of signal quenching by Cu^{2+} binding (green ≤15%; orange 15−25%; red ≥25%). The quenching is the average of that for all the observed ^{13}C sites for each residue. The arrows denote β-sheet regions reported in the previous studies by Tycko et al.[77]

perturbation from Cu^{2+} on the signal intensities. Similar signal quenching profile was obtained for Aβ(1−40) fibrils prepared at Dr. Tycko's lab at the NIH without agitation[70,76] (see the SI and Figure S3). Importantly, we also found that ^{13}C chemical shifts are not altered upon Cu^{2+} binding by more than 0.2 ppm for the hydrophobic core regions (residues 18−25 and 30−36) except for the moderate perturbation (∼0.35 ppm) on some sites of F19 and G33 (SI Table S1). The results provide the first crucial experimental evidence that Cu^{2+} binding does not reorganize or alter the parallel β-sheet structures of the hydrophobic core regions for Aβ(1−40) fibril with site resolution.

To identify other binding sites, we further performed 2D ^{13}C/^{13}C correlation SSNMR (Figure 3a) of *uniformly* ^{13}C- and ^{15}N-labeled Aβ(1−40) fibrils (black) without and (red) with Cu^{2+}. Surprisingly, as shown in the slices (Figure 3b−d), considerable signal quenching by 45 ± 11% and 59 ± 9% due to Cu^{2+} (orange arrows) was observed for $^{13}CO_2^-$ of (d) V40 in the C-terminus and (b) Glu sidechains, respectively. The extent of the quenching due to Cu^{2+} is comparable to those for His-13 and His-14. Although Glu signals were not assigned to individual residues, the results clearly suggest Cu^{2+} bindings to the carboxyl

dx.doi.org/10.1021/ja1072178 |*J. Am. Chem. Soc.* 2011, 133, 3390–3400

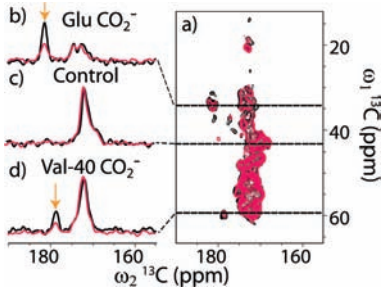

Figure 3. (a) 2D ^{13}C/^{13}C SSNMR spectra between aliphatic and ^{13}CO regions for uniformly ^{13}C- and ^{15}N-labeled Aβ(1−40) fibrils (black) without and (red) with Cu^{2+}, with 1D slices at ω_1 = (b) 34.6, (c) 43.9, and (d) 59.8 ppm. The spectra were obtained at a MAS of 40 kHz with an fpRFDR mixing of 1.6 ms.[87]

terminus of V40 and sidechains of Glu. Whereas binding to Glu was hypothesized in previous studies,[8] such Cu^{2+} binding, including that to the C-terminus, has been difficult to examine for Aβ fibrils until this work. Although site-directed mutations may be effective for short Aβ fragments,[29] such mutations on the full-length Aβ may alter the structure of amyloid fibril. The data in Figure 3a also indicate signals for other sidechain carboxyl groups at 175−180 ppm are likely quenched by Cu^{2+} binding; further studies will be needed for signal assignments and detailed analysis. With these SSNMR results, we conclude that the N-terminal region including H13, H14, and Glu sidechains and the CO_2^- in the C-termius are highly likely to play major roles in Cu^{2+} binding to the Aβ(1−40) fibril. The Cu^{2+} binding is likely to make very little or no changes on the basic structural units in the hydrophobic cores of the Aβ amyloid fibril.

To elucidate possible Cu^{2+} binding structures to Aβ, we performed two sets of MD simulations of Aβ(1−40) fibrils with Cu^{2+}. As the initial structure, we adopted a structural model from Tycko's group[77] with a fixed geometry for the residues 15−39 for oligomeric Aβ. In the first set of the MD simulation, we used cationic dummy atom (CaDa) approach for Cu^{2+} ions in order to identify possible Cu^{2+} binding ligands.[78] On the basis of our SSNMR results, Cu^{2+} ions were noncovalently bound to N_ε of H13 (or H14 in Figure 5) by ionic interactions in the initial structure. Indeed, the final structure with implicit solvents after three thermal annealing cycles demonstrated that CO^{2-}/CO sidechains of D1, E3, E11, Q15, and the CO_2^- terminal of V40 coordinate to Cu^{2+}, despite the absence of such interactions in the initial structures (Figure 4). While previous EPR studies for monomeric Aβ fragments[8,19,20,27] predicted two major coordination modes, here we suggest that a variety of coordination structures are likely to coexist in the amyloid fibril. Many of these observed binding modes are realized by the parallel β-sheet arrangements, in which Cu^{2+}-coordination sites at the N-terminal are concentrated via aggregation. For example, some Cu^{2+} ions were bridged by two H13 (or H14) rings of each two peptides (orange circles in Figures 4a and 5a). Such a binding mode is not possible in a monomer, although the possibility of Cu^{2+}-mediated intermolecular His bridge was proposed for an Aβ dimer previously.[69] Also, the Cu^{2+} ions bridge carboxyl terminal of V40 and H13 (or E11); such a binding has not been reported for monomeric Aβ. It should be noted that the above MD simulation results do not necessarily exclude the previously proposed coordination models by EPR and other studies. Our SSNMR results indeed indicate substantial relaxation on F4, which is consistent with the Cu^{2+} coordination to H6, which was

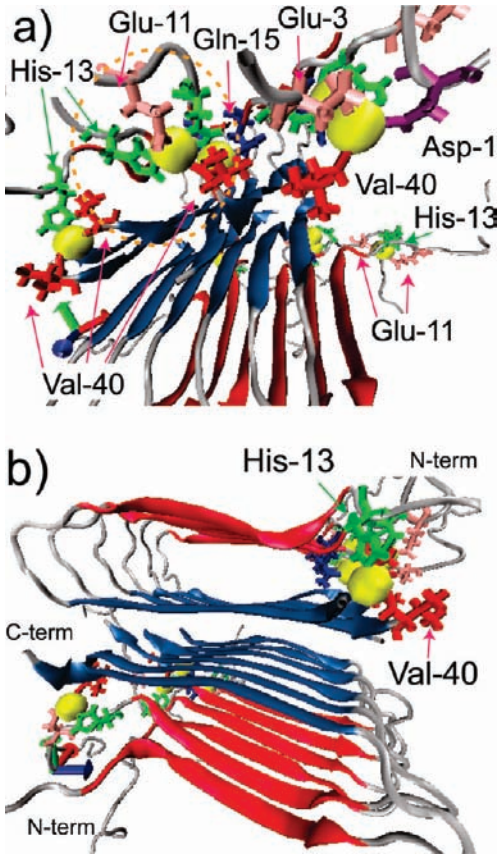

Figure 4. Final MD structure of Cu^{2+} bound Aβ(1−40) fibril viewed from (a) one of the N-terminal sides and (b) the fibril axis after three thermal annealing cycles (see the SI). In the initial structures, Cu^{2+} were bound to N_ε of H13 via noncovalent interactions. Blue and red arrows indicate β-sheet regions in residues 16−24 (red) and 30−39 (blue) of Aβ. The MD structure shows that Cu^{2+} (yellow) are bound to H13 (green), E3, E11 (pink), D1 (purple), Q15 (blue), and V40 (red) after the thermal cycles. The radius of the Cu^{2+} ion's sphere is ∼2 Å. The distances between Cu^{2+} and some of the ligands are shown in Figure S4 in the SI.

proposed by the previous EPR and NMR studies.[19,27,28] In our preliminary MD simulations in Figures 4 and 5, such long-range coordination may not be completely reproduced probably because of the restricted time frame of the simulations (20 ns) and the limited ensemble of the initial structures. Our MD simulation starting from a different initial structure with some Cu^{2+} ions coordinated to N_ε of H6, H13, H14 showed that a common Cu^{2+} ion can be coordinated to H6 and H14 of Aβ fibril (data not shown). It is possible that the various unique coordination modes presented here for the amyloid fibril coexist with those proposed for the monomeric/fragment Aβ at different population and perhaps in a dynamically exchangeable manner.[27]

To confirm the presence of various coordination modes, we examined the stability and the conformational energies for Aβ(1−40) fibril models of three different Cu^{2+}-binding modes (Table 1, Figure 6) with a more elaborate MD simulations using explicit solvents based on a recent study on Zn^{2+}−Aβ oligomer association.[68] The simulations show that such Cu^{2+}-coordination modes are all stable over 20 ns. In conformer 1, Cu^{2+} binds to His-6, His-13, and His-14 (Figure 6a), and in confomer 2, Cu^{2+} binds to Asp-1, His-6, and His-14 (Figure 6b). As shown in Table 1, conformer 1 (Figure 6a) is more stable than conformer 2 (Figure 6b); this indicates that the interaction of Cu^{2+} with His is

dx.doi.org/10.1021/ja1072178 |J. Am. Chem. Soc. 2011, 133, 3390–3400

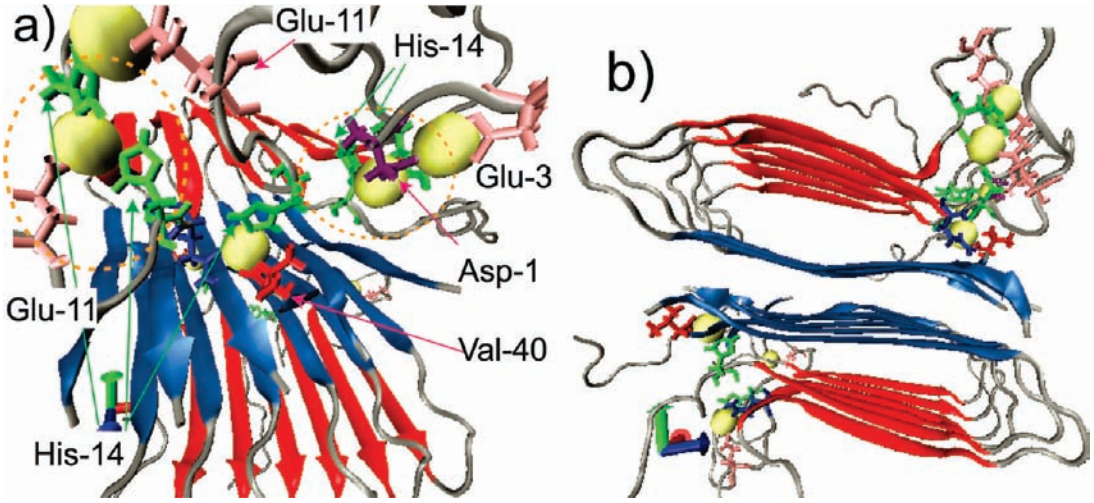

Figure 5. Final MD structure of Cu^{2+} bound Aβ(1−40) fibril viewed from (a) one of the N-terminal sides and (b) the fibril axis after three thermal annealing cycles. In the initial structures, Cu^{2+} were bound to N_ε of His-14 via noncovalent interactions. Blue and red arrows indicate β-sheet regions in residues 16−24 (red) and 30−39 (blue) of Aβ. The MD structure show that Cu^{2+} (yellow) are bound to His-14 (green), Glu-3, 11 (pink), Asp-1 (purple), Gln-15(blue), and Val-40 (red) after the thermal cycles. The radius of the yellow sphere is ∼2 Å from the Cu^{2+} ion.

likely to stabilize the model more than Asp, although the energy difference is within standard deviation due to thermal fluctuation. In conformer 3, 4 Cu^{2+} ions interact with D1, H6, and H14 and 4 Cu^{2+} ions bind to D1, H14, and V40 (Figure 6c); in conformer 4, the latter set of ligands are D1, H13, and V40 (Figure 6d). Conformer 4, which has Cu^{2+} coordination to $-CO_2^-$ of V40 and sidechains of D1 and H13, shows higher stability than conformer 2. The coordination of Cu^{2+} to D1, H14, V40 in conformer 3 also has a slightly higher stability than that of D1, H6, and H14 in conformer 2. These results suggest that Cu^{2+} may indeed interact with the C-termini, as suggested by our SSNMR analysis.

The simulations presented here are intended to provide insights into the possible ligands coordinated to Cu^{2+} in the Aβ amyloid fibril. At this point, universal force fields are not available for MD simulations involving Cu^{2+} ions.[18,79,80] Development of more optimized force fields is likely needed to reproduce more accurate coordination geometries for detailed comparison with EPR spectra. Despite the limitation, the MD simulation results allowed for the evaluation of Cu^{2+} coordination modes for more realistic Cu^{2+}−Aβ fibril model based on our SSNMR results, which suggested that the structural changes by Cu^{2+} binding are restricted to the N-term and C-term regions. It is encouraging that the two separate sets of MD simulations both suggested the previously unexpected unique coordination modes that are consistent with our SSNMR relaxation data.

In conclusion, this study has presented molecular details of Cu^{2+}-bound Aβ(1−40) amyloid fibril system by SSNMR. Three chemically and biologically novel aspects are presented in our work. First, this study has demonstrated the first systematic approach to examine binding of Cu^{2+} to insoluble amyloid aggregates at a site-specific level by SSNMR, based on the recent progress in SSNMR for small paramagnetic compounds[66,81−84] and for paramagnetic proteins[45,47,49,67] by our groups and other. We have shown that uses of paramagnetic quenching and chemical-shift perturbation in SSNMR can be effectively employed in order to examine possible Cu^{2+} binding sites and structural changes upon Cu^{2+} binding for insoluble amyloid system. Second, this study has, for the first time, provided

Table 1. Conformational Energy of Simulated Cu^{2+}−Aβ(1−40) Models

conformer	residues coordinated to Cu^{2+} [a]	conformational energy (kcal/mol) [b]
1	H6, H13, H14	−11978.1 (205.2)
2	D1, H6, H14	−11857.3 (171.5)
3	D1, H6, H14 and D1, H14, V40	−11873.9 (164.5)
4	D1, H6, H14 and D1, H13, V40	−11901.7 (185.0)

[a] See Figure 6 for the modes of the coordination for each conformer. [b] Conformational energies were computed using the GBMV calculations.[103] The conformational energy is the total energy of the oligomer including the 8 Aβ molecules and the copper ions. Standard deviation values are in parentheses.

detailed site-specific structural information on Cu^{2+} bound full-length Aβ(1−40) in amyloid fibrils. Despite the linkage of the Cu^{2+}−Aβ fibril with AD and its significance as a potential pharmaceutical target,[14−16] Cu^{2+}−Aβ association has been examined mostly for smaller and early stage model systems such as soluble Aβ fragments or Aβ monomers. Our study has offered a solution to this situation by overcoming the difficulties in the sample preparation and the lack of suitable structural analysis methods for Cu^{2+}−Aβ in amyloid fibrils, for which structural information has been very scarce. Third, our SSNMR data experimentally demonstrated various novel features of Cu^{2+} coordination to the Aβ fibril. Besides offering experimental evidence of the Cu^{2+} coordination to N_ε of H13 and H14, this study has revealed previously unexpected ligands such as the carboxyl group of V40 at the C-terminus and Glu sidechains. Our chemical-shift perturbation data suggested very little structural changes for the hydrophobic core regions (residues 18-25 and 30−36) of the Aβ fibrils upon Cu^{2+} binding. The unique coordination modes suggested by SSNMR were confirmed by the two sets of MD simulations on sophisticated Aβ oligomer models reflecting realistic amyloid fibril structures. Unlike previous MD studies on Cu^{2+}−Aβ binding,[18] both MD simulations incorporated intermolecular parallel β-sheet structure that is characteristic of the Aβ(1−40) amyloid fibril as well as the

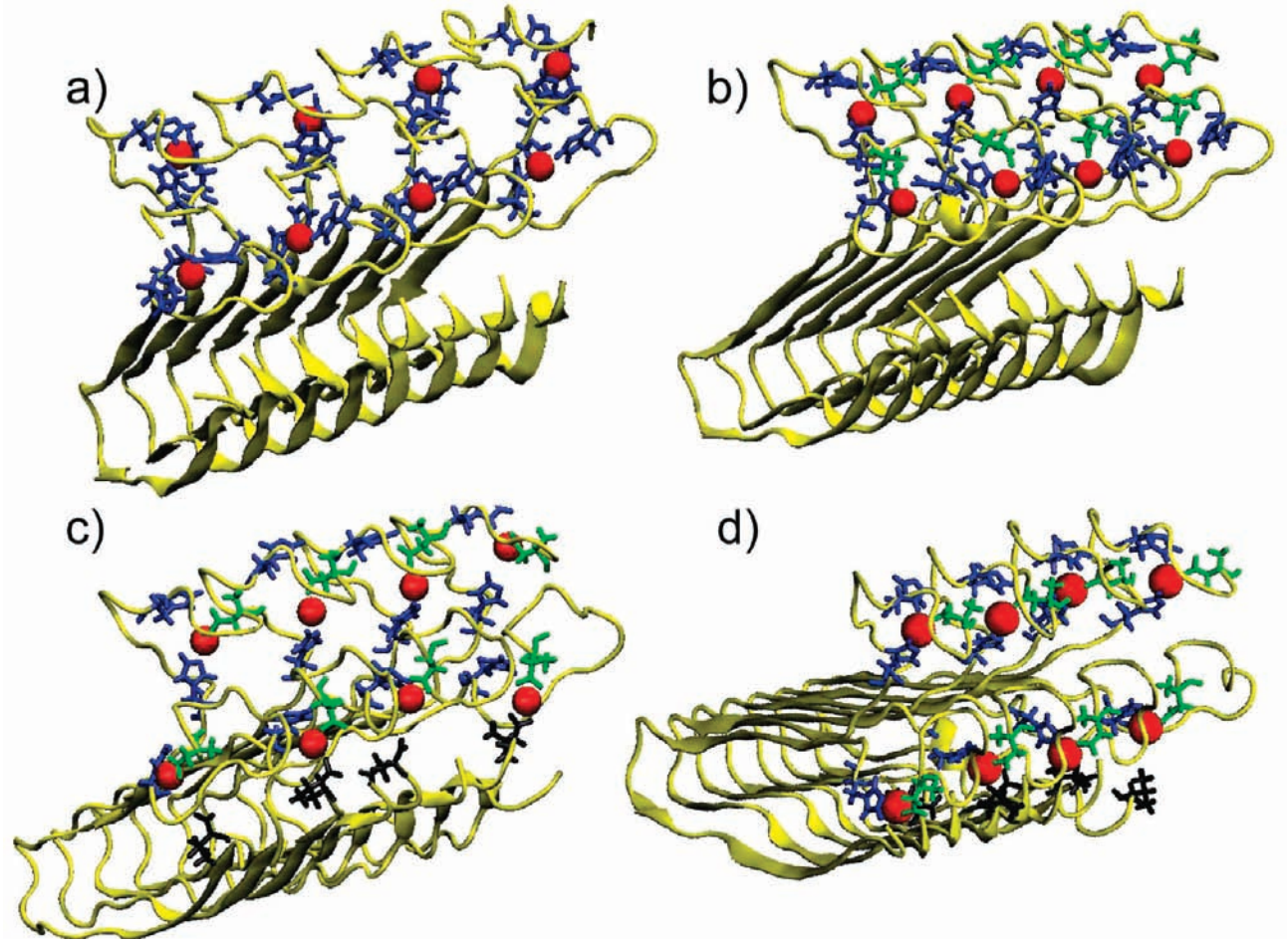

Figure 6. (a) Conformer 1 for which His-6, His-13, and His-14 residues are coordinated to copper ions. (b) Conformer 2 for which Asp-1 (green), His-6 (blue), and His-14 (blue) residues are coordinated to a copper ion. (c) Conformer 3 for which Asp-1 (green), His-6 (blue), and His-14 (blue) residues are coordinated to a copper ion and Asp-1 (green), His-14 (blue), and Val-40 (black) are coordinated to another copper ion. (d) Conformer 4 for which Asp-1 (green), His-6 (blue), and His-14 (blue) residues are coordinated to a copper ion and Asp-1 (green), His-13 (blue), and Val-40 (black) are coordinated to another copper ion. The magnified coordination geometries are shown in Figure S6 in the SI.

nonconvalent bonding models for Cu^{2+}−ligand interactions. Although further studies are needed to fully understand Cu^{2+} binding structure to Aβ, including its relation to the previous EPR studies and a ROS production mechanism, the combination of SSNMR analyses and MD simulations have provided insights into previously unknown detailed structural features of Cu^{2+}-bound Aβ(1−40) in amyloid fibrils.

The new SSNMR approach presented here may be also applicable to examine binding of small paramagnetic ligands, such as drugs, to amyloid proteins. It has been proposed that metal ions such as Cu^{2+} and Zn^{2+} may trigger the formation of Aβ oligomer or fibril, modulating misfolding kinetics and aggregation states of Aβ.[25,30,85] In this initial work, we focused on establishing SSNMR structural analysis of Aβ(1−40) fibril upon Cu^{2+} binding after fibril formation. A similar approach is likely useful for SSNMR characterization of the structures of Aβ oligomer and Aβ fibril that are formed in the presence of Cu^{2+} or other metal ions.

MATERIALS AND METHODS

Synthesis and Purification of Aβ(1−40) Peptide. Aβ(1−40) peptide (NH2-DAEFRHDSGY-EVHHQKLVFF-AEDVGSNKGA-IIGLMVGGVV-COOH) was synthesized and purified as reported previously. Briefly, Aβ(1−40) was synthesized using solid-phase peptide synthesis with standard Fmoc synthesis and cleavage protocols.[40,76] The crude peptide was purified by HPLC using acetonitrile and water gradient with 0.1% trifluoroaceticacid. ^{13}C- and ^{15}N-labeling was introduced as described previously by incorporating Fmoc-protected uniformly ^{13}C- and ^{15}N-labeled amino acids at selected residues. The Fmoc protection of the uniformly ^{13}C- and ^{15}N-labeled amino acids (Isotec/Sigma-Aldrich, Miamisburg, OH) was performed at the Research Resource Center (RRC) at the University of Illinois at Chicago (UIC) using the protocol of Fields et al.[86] The purities of the peptide samples were determined by MALDI-TOF mass spectra performed at UIC RRC, and the purities were approximately 95% after the HPLC purification. The purified samples were stored at −20 °C before they were used. The labeling schemes for the six samples used are as follows: (1) His-14, Ile-32, Val-36, Gly-37; (2) His-13, Ala-30, Gly-38, Val-39; (3) Val-12, Phe-20, Ala-21, Ile-31,Gly-33, Met-35($^{13}C_{\varepsilon}H_3$); (4) Phe-4, Gly-9, Val-12, Leu-17, Ala-21; (5) Phe-19, Val-24, Gly-25, Ala-30, Leu-34; (6) Val-18, Phe-19, Ala-21, Ile-31, Gly-33.

Uniformly ^{13}C- and ^{15}N-labeled Aβ(1−40) was expressed as a fusion protein with Glutathione S-Transferase (GST) tag connected by a Factor Xa recognition site (IEGR$^{\blacktriangledown}$) in *E. coli*. The GST tag was removed by Factor Xa enzymatic cleavage, and then,

the peptide was purified by HPLC as described above. The yield of uniformly ^{15}N- and/or ^{13}C-protein Aβ(1−40) was ∼1.5 mg from 1 L of the cell culture. The details of the protocol will be discussed elsewhere.

Preparation of Aβ(1−40) Fibrils for Cu^{2+}-Binding Assay and SSNMR Experiments. For Cu^{2+}-binding assay with Aβ(1−40) fibrils using UV−vis spectroscopy, a solution of 5 mM Aβ(1−40) was prepared by first dissolving Aβ(1−40) peptide in 50 mM NaOH.[45] The peptide mixture was then briefly vortexed and diluted to a final peptide concentration of 500 μM with deionized water containing 0.02% NaN_3. The pH of the solution was adjusted to 7.4 by using 100 mM HCl. The Aβ(1−40) solution was sonicated for 5 min in an ice bath, and this solution was then centrifuged at 16.1 × 10^3*g* for 5 min to remove any preformed aggregates. The peptide solution was divided into several 1.5 mL microvials for Cu^{2+}-binding assay. The concentration of Aβ(1−40) was measured using UV−vis spectroscopy.[40] The Aβ(1−40) solution was then incubated for 14 days with constant agitation in the sample tube at room temperature. Aβ(1−40) fibril formation was confirmed by thioflavin T (ThT) fluorescence assay.

For SSNMR studies, amyloid fibril samples were prepared as described above, but with selectively isotope-labeled or uniformly ^{13}C- and ^{15}N-labeled Aβ(1−40) peptides. For the samples used for Figures 1 and 2, after incubation of an Aβ solution for fibril formation, the Aβ(1−40) fibril with Cu^{2+} was prepared by adding $CuCl_2$ solution (pH7.4) to the Aβ solution in the mole ratio of 0.4:1.0 (Cu^{2+}:Aβ(1−40)) and incubated at 4 °C for 24 h with initial vortexing. The control sample without Cu^{2+} was prepared in the same manner except for the addition of $CuCl_2$. The samples were then centrifuged at 16.1 × 10^3*g* for about 1 h (20 min at a time), and the supernatant was removed. The gel-like pellet at the bottom was then lyophilized. The lyophilized Aβ(1−40) fibril samples with and without Cu^{2+} were packed in to 2.5 mm MAS rotors with rubber O-rings on the spacer and cap. The lyophilized samples were rehydrated with deionized water (3 μL water/mg Aβ(1−40)) in the rotor with 3 μL of water added at one time and centrifuged at 2.0 × 10^3*g* for 2 min. The hydrated samples were incubated overnight at 4 °C before running the SSNMR experiments.

For the uniformly ^{13}C- and ^{15}N-labeled Aβ(1−40) fibril sample used for Figure 3, after incubation for fibril formation, we centrifuged the sample at 16.1 × 10^3*g* for ∼1.0 h (20 min at a time) and removed the supernatant. The gel-like pellet at the bottom of the centrifugal vial was transferred into the 1.8 mm MAS rotor of 10 μL volume by centrifugation. The fibrils were then packed into a 1.8 mm rotor by fitting a 200 μL pipet tip to the rotor with the fibrils and centrifuging the rotor pipet tip mounted in a microcentrifuge tube with a minimum amount of the supernatant for 2−4 min at 6 × 10^3*g*. Then, the rotor cap was glued with Krazy Glue (Krazy Glue, Columbus OH) with a small piece of Teflon tape between the cap and the sample to avoid interaction of the glue with the peptide. This cap can be removed easily by immersing it in liquid nitrogen. The Aβ(1−40) fibrils with Cu^{2+} was prepared by adding a 26.5 mM $CuCl_2$ solution in the mole ratio of 0.4:1.0 (Cu^{2+}:Aβ(1−40)) into the rotor. First, the hydrated Aβ(1−40) sample in a rotor was lyophilized, and then a $CuCl_2$ solution was introduced directly into the 1.8 mm rotor by centrifugation and the cap was glued as described above. The rotor was then incubated at 4 °C for 24 h before the SSNMR experiments.

SSNMR Experiments. All the SSNMR experiments were performed with an Infinityplus SSNMR spectrometer from Varian (Fort Collins, CO) with a home-built 2.5 mm MAS triple-resonance magic-angle spinning (MAS) probe or a 1.8 mm MAS triple-resonance MAS probe developed at Dr. Samoson's lab (National Institutes of Chemical Physics and Biophysics, Tallinn, Estonia) at 9.4 T (^{1}H frequency of 400.2 MHz) in the double-configuration. For the data in Figures 1 and 2, the spinning speed was set to 20 000 ± 3 Hz throughout the experiments with cooling air at −10 °C supplied through a Varian VT stack at a flow rate of ∼140 standard cubic feet per hour (scfh), which kept the sample temperature at ∼11 °C. Approximately, 2.0−3.5 mg of labeled Aβ(1−40) fibril samples were used. In the 1D ^{13}C CPMAS experiments for Figures 1 and 2, adiabatic CP transfer was used. During the CP period, the ^{13}C RF field amplitude was linearly swept from 45−65 kHz during a contact time of 1.0 ms while the ^{1}H RF amplitude was kept constant at 75 kHz. During the detection period, ^{1}H TPPM decoupling of 90 kHz was employed. The recycle delays for the 1D experiments were 1.8 s. The 1D spectra in Figures 1c and 2c were collected with 1024 scans and were processed with Gaussian broadening of 20 and 150 Hz, respectively. The 1D spectra in Figure 2a and b were collected with 4096 scans and processed with Gaussian broadening of 150 Hz.

In the 2D experiments for Figure 1d, a 2D ^{13}C/^{13}C correlation pulse sequence with the fpRFDR (finite-pulse radio-frequency-driven dipolar recoupling) mixing was used.[76,87] After the adiabatic CP, signals were recorded during the t_1 period, and then a real or imaginary component of the magnetization was stored along the *z* axis. Then, during a mixing period, a fpRFDR ^{13}C/^{13}C dipolar-recoupling sequence with a mixing time of 1.6 ms and a ^{13}C π-pulse width of 15 μs was used. ^{1}H TPPM decoupling of 90 kHz was employed during the t_1 and t_2 periods, while cw decoupling of the same amplitude was used during the mixing period. For each t_1 point, 192 scans of signals were accumulated with an acquisition period of 10 ms. A total of 180 complex t_1 points were recorded with a t_1 increment of 33.4 μs. The obtained NMR data were processed by NMRPipe software.[88] Gaussian window functions of 110 and 90 Hz were applied along the t_1 and t_2 time domains. An overall experimental time was 35 h. The experiments were performed for the six Aβ samples listed above in which different residues are uniformly ^{13}C- and ^{15}N-labeled. ^{15}N-labeling was introduced for experiments to be performed in the future.

The spectra in Figure 3 were acquired at a spinning speed of 40 000 ± 10 Hz with cooling air at −20 °C supplied through a Varian VT stack at a flow rate of ∼140 scfh with cooled bearing air (1 °C), which kept sample temperature at ∼12 °C. The 2D ^{13}C/^{13}C correlation spectra were obtained using fpRFDR mixing of 1.6 ms with ^{13}C π- pulse widths of 13 μs. Approximate amount of the Aβ fibril sample (excluding water) was ∼0.6 mg. The π/2-pulse for proton excitation was 2.5 μs. During the 1 ms CP period, the ^{13}C rf field was swept from 48−76 kHz, while the ^{1}H rf field was kept at 102 kHz. The signal was collected during an acquisition period of 10 ms with low-power TPPM (lpTPPM) ^{1}H decoupling while the rf field intensity ($\omega_1/2\pi$) at 7 kHz was applied with phase alternation between ±17°. A total of 126 complex t_1 points were recorded with a t_1 increment 48 μs. For each t_1 point, 728 scans of signals were accumulated. For the uniformly ^{13}C- and ^{15}N-labeled Aβ fibril sample without Cu^{2+}, total experimental time was 72 h with recycle delays of 1.4 s. For the sample with 0.4 mol equiv of Cu^{2+}, the experiment was collected using PACC method[45] with a total experimental time of 8 h and recycle delays of 150 ms. The details of the pulse program and lpTPPM are described elsewhere.[45,89] The obtained NMR data were processed by NMR pipe software. Lorentz to Gaussian window functions with inverse exponential width of 30 Hz

and Gaussian broadening of 80 Hz were applied for both t_1 and t_2 time domains.

Molecular Dynamics (MD) Simulations Protocol. In order to identify possible Cu^{2+} binding structures in Aβ(1−40) fibrils and verify their structural stabilities, we have performed two sets of molecular dynamics (MD) simulations. In the first set of the MD simulations related to the structure shown in Figures 4−5, we used the structural refinement within AMBER 8.[90] MD simulations were performed using a modified AMBER ff99sb force field[91] with generalized Born (GB) implicit solvation[92] on an Argo Beowulf PC cluster at the Academic Computing and Communications Center at UIC (http://www.uic.edu/depts/accc/hardware/argo/index.html). The AMBER refinement scheme used herein is a slightly modified version which has been used for a number of NMR structure refinements.[93] Force-fields for Cu^{2+} were adopted from those for Zn^{2+} denoted as *tetrahedral divalent cation* model and used with a minor modification with the differences in the atomic mass (65.360) and Van der waals (VDW) radius for copper (r^* = 3.100 Å).[78] Although it is possible that Cu^{2+} bound to Aβ takes other coordinates such as a distorted planar geometries suggested by EPR studies,[19,21] we assumed this tetrahedral geometry in order to identify possible metal binding structures for one of the most common Cu^{2+} geometries. It is interesting to note, however, that for the *undistorted* tetrahedral model of Cu^{2+} used herein, the ligands can readily sample and coordinate in a distorted fashion (SI Table S2). Thus, there is indeed some flexibility with regard to how the ligands can arrange around the Cu ions in the CaDa model. In a recent study to simulate Cu^{2+}-binding to Aβ(1−40), Baik et al. showed that the optimization of Cu^{2+} coordination to His by ab initio calculations resulted in the distorted tetrahedral symmetry.[18] A comparison of the coordination geometries for the MD structures for Cu, Zn-superoxide dismutase (SOD) obtained with different types of force fields with X-ray structure showed that the structural parameters obtained by the tetrahedral model show reasonable agreement with those for the X-ray structure (see Table S2 in the SI). A recent X-ray study suggested that Cu, Zn SOD, a type II Cu^{2+} protein, which has a distorted square-planar Cu^{2+} coordination geometry, shows very limited changes in the coordination structure by replacement of Cu^{2+} with Zn^{2+} (i.e., Zn, Zn SOD).[94] This is consistent with our MD simulation results with the Cu−CaDa tetrahedral model in the SI. The initial structure of the Aβ(1−40) fibril was adopted from Tycko's model,[77] and the missing eight N-terminal amino acids were built back into the molecule using Molmol.[95] On the basis of our NMR data, two sets of initial Cu^{2+} locations (i.e., at His-13 or His-14) were assumed; Cu^{2+} was noncovalently attached to N_ε of His-13 for Figure 4 (or His-14 for Figure 5) by replacement of the H_ε and held in position by the incorporation of an NOE between the Cu^{2+} atom and N_ε of His with a square well potential varying from 1.6 to 3.0 Å and a force constant of 10 kcal/mol. Protons at the N_δ positions of Cu^{2+}-bound His-13/14 were removed, while those for other histidines were retained. All hydrogen atom bond lengths were constrained using the SHAKE algorithm.[96] A cutoff of 12 Å was used for nonbonded interactions. Steepest descentminimization was performed for 2000 steps prior to and after MD refinement. The final MD structures were obtained after three thermal annealing cycles (0 → 1000 → 0 K) for a total of 60 ps run time. During the MD simulations, the coordinates of residues 16−39 were fixed using a harmonic potential of 20 kcal/mol. Based on our NMR results, the structure of these regions is likely to be unaffected by Cu^{2+}-binding. As shown in Figure 4a and Figure 5a, respectively, many Cu^{2+} ions remained attached to His-13 and His-14 via ionic interactions even after three thermal cycles, while some ions dissociated from the positions. Although previous EPR studies predicted only two major Cu^{2+} binding structures, coexistence of a variety of binding modes was observed in our MD simulations. The simulations provided insights into the possible metal binding structures.

The second set of MD simulations in Figure 6 was used to rigorously compare the stability of the Cu^{2+} binding structures for three possible binding modes. For the conformation energy calculations in Table 1, MD simulations of solvated 8Cu^{2+}−Aβ(1−40) oligomers were also performed in the NPT ensemble using the NAMD program[97] and the CHARMM package[98] with the all-atom CHARMM27 force field. The oligomers were explicitly solvated with TIP3P water molecules. Constant temperature (300 K) and constant pressure (1 atm) were controlled by a Langevin thermostat with a damping coefficient of 10 ps^{-1}, using the NAMD program. For simulations using the NAMD program,[97] the Langevin piston method[97,99,100] with a decay period of 100 fs, and a damping time of 50 fs was used to maintain a constant pressure of 1 atm. The short-range VDW interactions were calculated using the switching function, with a twin range cutoff of 10.0 and 12.0 Å. Long-range electrostatic interactions were calculated using the particle mesh Ewald method with a cutoff of 12.0 Å for all simulations. The equations of motion were integrated using the leapfrog integrator with a step of 1 fs. All initial 8Cu^{2+}−Aβ(1−40) oligomer was minimized and then solvated in a TIP3P water box with a minimum distance of 15 Å from any edge of the box to any Aβ atom. Any water molecule within 2.5 Å of the Aβ was removed. Even with Cu^{2+} binding, the overall charge for Cu^{2+}−Aβ(1−40) is still −1. Therefore, counterions (Na^+) were added into solution at random locations to neutralize the charge of Cu^{2+}−Aβ(1−40). The solvated systems were minimized for 2000 conjugated gradient steps, with the distance between the β-sheets fixed in the range 2.2−2.5 Å. The VDW parameters of Cu^{2+} ion and all Cu^{2+}-ligands distances were constrained to the estimated distances,[101] both along the minimization process and during all dynamics simulation time scales. Counter ions, peptides, and water molecules were all allowed to move. The hydrogen atoms were constrained to the equilibrium bond using the SHAKE algorithm.[96] The minimized solvated systems were quickly heated to 250 K, where all atoms were allowed to move. Then, the systems were heated from 250 to 300 K for 300 ps and equilibrated at 300 K for 300 ps. Simulations ran for 20 ns and structures were saved every 10 ps for analysis.

A copper-binding octamer was constructed from Tycko's amyloid fibril model.[77] We used one monomer from the fibril conformation of Aβ(9−40). Residues G9-K16 were removed from each monomer and the N-terminal fragment peptide (D1-K16) was linked binding to Cu^{2+}. The initial conformation of Cu^{2+}−Aβ(1−16) was combined with the Aβ(17−40) as follows. The Zn^{2+} ions in the solution NMR structure of Zn^{2+}−Aβ(1−16) complex from the work of Zirah et al.[102] were replaced with the Cu^{2+} ion. Then, all Cu^{2+}-ligands distances were constrained to the estimated distances with the residues that coordinate with the ions. On the basis of previous EPR and NMR studies,[19−21,27] two conformers were tested where Cu^{2+} binds to residues in the N-terminal: in the first model, Cu^{2+} binds to H6, H13, and H14 (conformer 1; Figure 6a) and, in the second model, Cu^{2+} interacts with D1, H6, and H14 (conformer 2; Figure 6b). To test interactions of the copper ions with the C-termini of Aβ suggested in the SSNMR data and CaDa MD

simulation, we constructed a model with 4 Cu^{2+} ions coordinating to D1, H14, and V40 and 4 Cu^{2+} ions to D1, H6, and H14 (conformer 3; Figure 6c) and another model with 4 Cu^{2+} ions coordinating to D1, H14, and V40 and 4 Cu^{2+} ions to D1, H6, and H13 (conformer 4; Figure 6d).

Analysis Details for MD Simulations. To obtain the relative structural stability of the $8Cu^{2+}$−Aβ(1−40) oligomers listed in Table 1, the Aβ trajectories of the last 5 ns were first extracted from the explicit MD simulation excluding water molecules. The solvation energies of all systems were calculated using the Generalized Born Method with Molecular Volume (GBMV).[103,104] In the GBMV calculations, the dielectric constant of water was set to 80.0 and no distance cutoff was used. The hydrophobic solvent-accessible surface area (SASA) term factor was set to 0.00592 kcal/mol·Å^2. Each conformer is minimized for 1000 cycles, and the conformation energy is evaluated by grid-based GBMV. The minimization does not change the conformations of each conformer but only relaxed the local geometries due to thermal fluctuation which occurred during the MD simulations.

The relative conformational stabilities of the oligomers were measured by root mean-squared deviation (RMSD) of the C-terminal region (residues Leu17−Val40), the N-terminal region (residues Ala2−Gln15), and for the U-turn region (residues Glu22−Gly29) with respect to the initial minimized structure throughout the simulations. We also examined the stability of the oligomers by following changes in the number of hydrogen bonds between the β strands with the hydrogen bond cutoff set to 2.5 Å (SI Figure S7a) and by monitoring the change in the intersheet distance (Cα backbone−backbone distance) in the core domains of all oligomers (Ala21−Ile31 distance; SI Figure S7b). The latter distance is the averaged distance between each two β-sheet regions near to the salt bridge in each monomer for each conformer.

■ ASSOCIATED CONTENT

Supporting Information. Details of sample preparation, Cu^{2+} binding assays, and other SSNMR and MD data. This material is available free of charge via the Internet at http://pubs.acs.org.

■ AUTHOR INFORMATION

Corresponding Author
yishii@uic.edu

■ ACKNOWLEDGMENT

This study was supported primarily by NIH RO1 program (AG028490) and the Alzheimer's Association grant (IIRG 08-91256). The SSNMR methodology development in this work was also supported by the NSF (CHE 449952, CHE 957793) and the Dreyfus Foundation Teacher-Scholar Award program. This project has been funded in part with Federal funds from the NCI, NIH, under contract number HHSN261200800001E. Simulations were also performed on the Biowulf cluster at the NIH (http://biowulf.nih.gov). We thank Dr. Robert Tycko at the NIH for providing a pdb file of the structural model for Aβ(1−40) fibril and the Aβ fibrils samples used for Figure S3 in the SI. We are also grateful to Prof. Michael Zagorski at Case Western Reserve University for kind clarifications on his works.

■ REFERENCES

(1) Mattson, M. P. *Nature* **2004**, *430*, 631–639.
(2) Selkoe, D. J. *Nat. Cell Biol.* **2004**, *6*, 1054–1061.
(3) Lovell, M. A.; Robertson, J. D.; Teesdale, W. J.; Campbell, J. L.; Markesbery, W. R. *J. Neurol. Sci.* **1998**, *158*, 47–52.
(4) Leskovjan, A. C.; Lanzirotti, A.; Miller, L. M. *Neuroimage* **2009**, *47*, 1215–1220.
(5) Miller, L. M.; Wang, Q.; Telivala, T. P.; Smith, R. J.; Lanzirotti, A.; Miklossy, J. *J. Struct. Biol.* **2006**, *155*, 30–37.
(6) Huang, X. D.; Atwood, C. S.; Hartshorn, M. A.; Multhaup, G.; Goldstein, L. E.; Scarpa, R. C.; Cuajungco, M. P.; Gray, D. N.; Lim, J.; Moir, R. D.; Tanzi, R. E.; Bush, A. I. *Biochemistry* **1999**, *38*, 7609–7616.
(7) Ali, F. E.; Separovic, F.; Barrow, C. J.; Cherny, R. A.; Fraser, F.; Bush, A. I.; Masters, C. L.; Barnham, K. J. *J. Pept. Sci.* **2005**, *11*, 353–360.
(8) Faller, P. *Chembiochem* **2009**, *10*, 2837–2845.
(9) Opazo, C.; Huang, X. D.; Cherny, R. A.; Moir, R. D.; Roher, A. E.; White, A. R.; Cappai, R.; Masters, C. L.; Tanzi, R. E.; Inestrosa, N. C.; Bush, A. I. *J. Biol. Chem.* **2002**, *277*, 40302–40308.
(10) Scott, L. E.; Orvig, C. *Chem. Rev.* **2009**, *109*, 4885–4910.
(11) Atwood, C. S.; Scarpa, R. C.; Huang, X. D.; Moir, R. D.; Jones, W. D.; Fairlie, D. P.; Tanzi, R. E.; Bush, A. I. *J. Neurochem.* **2000**, *75*, 1219–1233.
(12) Atwood, C. S.; Moir, R. D.; Huang, X. D.; Scarpa, R. C.; Bacarra, N. M. E.; Romano, D. M.; Hartshorn, M. K.; Tanzi, R. E.; Bush, A. I. *J. Biol. Chem.* **1998**, *273*, 12817–12826.
(13) Bush, A. I.; Tanzi, R. E. *Proc. Natl. Acad. Sci. U. S. A.* **2002**, *99*, 7317–7319.
(14) Bush, A. I. *J. Alz. Dis.* **2008**, *15*, 223–240.
(15) Barnham, K. J.; Kenche, V. B.; Ciccotosto, G. D.; Smith, D. P.; Tew, D. J.; Liu, X.; Perez, K.; Cranston, G. A.; Johanssen, T. J.; Volitakis, I.; Bush, A. I.; Masters, C. L.; White, A. R.; Smith, J. P.; Cherny, R. A.; Cappai, R. *Proc. Natl. Acad. Sci. U.S.A.* **2008**, *105*, 6813–6818.
(16) Choi, J.-S.; Braymer, J. J.; Nanga, R. P. R.; Ramamoorthy, A.; Lim, M. H. *Proc. Natl. Acad. Sci. U.S.A.* **2010**, *107*, 21990–21995.
(17) Jun, S.; Gillespie, J. R.; Shin, B.-k.; Saxena, S. *Biochemistry* **2009**, *48*, 10724–10732.
(18) Mantri, Y.; Fioroni, M.; Baik, M. H. *J. Biol. Inorg. Chem.* **2008**, *13*, 1197–1204.
(19) Drew, S. C.; Noble, C. J.; Masters, C. L.; Hanson, G. R.; Barnham, K. J. *J. Am. Chem. Soc.* **2009**, *131*, 1195–1207.
(20) Drew, S. C.; Masters, C. L.; Barnham, K. J. *J. Am. Chem. Soc.* **2009**, *131*, 8760–8761.
(21) Sarell, C. J.; Syme, C. D.; Rigby, S. E. J.; Viles, J. H. *Biochemistry* **2009**, *48*, 4388–4402.
(22) Minicozzi, V.; Stellato, F.; Comai, M.; Serra, M. D.; Potrich, C.; Meyer-Klaucke, W.; Morante, S. *J. Biol. Chem.* **2008**, *283*, 10784–10792.
(23) Ali, F. E.; Separovic, F.; Barrow, C. J.; Yao, S. G.; Barnham, K. J. *Int. J. Pept. Res. Ther.* **2006**, *12*, 153–164.
(24) Gaggelli, E.; Grzonka, Z.; Kozlowski, H.; Migliorini, C.; Molteni, E.; Valensin, D.; Valensin, G. *Chem. Commun.* **2008**, 341–343.
(25) Lim, K. H.; Kim, Y. K.; Chang, Y. T. *Biochemistry* **2007**, *46*, 13523–13532.
(26) Miura, T.; Suzuki, K.; Kohata, N.; Takeuchi, H. *Biochemistry* **2000**, *39*, 7024–7031.
(27) Hou, L. M.; Zagorski, M. G. *J. Am. Chem. Soc.* **2006**, *128*, 9260–9261.
(28) Karr, J. W.; Kaupp, L. J.; Szalai, V. A. *J. Am. Chem. Soc.* **2004**, *126*, 13534–13538.
(29) Karr, J. W.; Szalai, V. A. *J. Am. Chem. Soc.* **2007**, *129*, 3796-.
(30) Liu, S. T.; Howlett, G.; Barrow, C. J. *Biochemistry* **1999**, *38*, 9373–9378.
(31) Antzutkin, O. N. *Magn. Reson. Chem.* **2004**, *42*, 231–246.
(32) Hindo, S. S.; Mancino, A. M.; Braymer, J. J.; Liu, Y. H.; Vivekanandan, S.; Ramamoorthy, A.; Lim, M. H. *J. Am. Chem. Soc.* **2009**, *131*, 16663.
(33) Olofsson, A.; Lindhagen-Persson, M.; Vestling, M.; Sauer-Eriksson, A. E.; Ohman, A. *Febs J.* **2009**, *276*, 4051–4060.

(34) Zoroddu, M. A.; Medici, S.; Peana, M. *J. Inorg. Biochem.* **2009**, *103*, 1214–1220.
(35) Karr, J. W.; Szalai, V. A. *Biochemistry* **2008**, *47*, 5006–5016.
(36) Petkova, A.; Ishii, Y.; Balbach, J. J.; Antzutkin, O. N.; Leapman, R. D.; Delaglio, F.; Tycko, R. *Proc. Natl. Acad. Sci. U.S.A.* **2002**, *99*, 16742–16747.
(37) Heise, H.; Hoyer, W.; Becker, S.; Andronesi, O. C.; Riedel, D.; Baldus, M. *Proc. Natl. Acad. Sci. U.S.A.* **2005**, *102*, 15871–15876.
(38) Chimon, S.; Ishii, Y. *J. Am. Chem. Soc.* **2005**, *127*, 13472–13473.
(39) Sciarretta, K. L.; Gordon, D. J.; Petkova, A. T.; Tycko, R.; Meredith, S. C. *Biochemistry* **2005**, *44*, 6003–6014.
(40) Chimon, S.; Shaibat, M. A.; Jones, C. R.; Calero, D. C.; Aizezi, B.; Ishii, Y. *Nat. Struct. Mol. Biol.* **2007**, *14*, 1157–1164.
(41) Wasmer, C.; Soragni, A.; Sabate, R.; Lange, A.; Riek, R.; Meier, B. H. *Angew. Chem., Int. Ed.* **2008**, *47*, 5839–5841.
(42) Helmus, J. J.; Surewicz, K.; Nadaud, P. S.; Surewicz, W. K.; Jaroniec, C. P. *Proc. Natl. Acad. Sci. U.S.A.* **2008**, *105*, 6284–6289.
(43) Curtis-Fisk, J.; Spencer, R. M.; Weliky, D. P. *J. Am. Chem. Soc.* **2008**, *130*, 12568.
(44) Jaroniec, C. P.; MacPhee, C. E.; Astrof, N. S.; Dobson, C. M.; Griffin, R. G. *Proc. Natl. Acad. Sci. U.S.A.* **2002**, *99*, 16748–16753.
(45) Wickramasinghe, N. P.; Parthasarathy, S.; Jones, C. R.; Bhardwaj, C.; Long, F.; Kotecha, M.; Mehboob, S.; Fung, L. W. M.; Past, J.; Samoson, A.; Ishii, Y. *Nat. Meth.* **2009**, *6*, 215–218.
(46) Masuda, Y.; Uemura, S.; Ohashi, R.; Nakanishi, A.; Takegoshi, K.; Shimizu, T.; Shirasawa, T.; Irie, K. *Chembiochem* **2009**, *10*, 287–295.
(47) Pintacuda, G.; Giraud, N.; Picrattelli, R.; Bockmann, A.; Bertini, I.; Emsley, L. *Angew. Chem., Int. Ed.* **2007**, *46*, 1079–1082.
(48) Balayssac, S.; Bertini, I.; Lelli, M.; Luchinat, C.; Maletta, M. *J. Am. Chem. Soc.* **2007**, *129*, 2218–2219.
(49) Balayssac, S.; Bertini, I.; Bhaumik, A.; Lelli, M.; Luchinat, C. *Proc. Natl. Acad. Sci. U.S.A.* **2008**, *105*, 17284–17289.
(50) Pooransingh-Margolis, N.; Renirie, R.; Hasan, Z.; Wever, R.; Vega, A. J.; Polenova, T. *J. Am. Chem. Soc.* **2006**, *128*, 5190–5208.
(51) Castellani, F.; van Rossum, B.; Diehl, A.; Schubert, M.; Rehbein, K.; Oschkinat, H. *Nature* **2002**, *420*, 98–102.
(52) Morcombe, C. R.; Gaponenko, V.; Byrd, R. A.; Zilm, K. W. *J. Am. Chem. Soc.* **2005**, *127*, 397–404.
(53) Lorieau, J. L.; Day, L. A.; McDermott, A. E. *Proc. Natl. Acad. Sci. U.S.A.* **2008**, *105*, 10366–10371.
(54) Qiang, W.; Bodner, M. L.; Weliky, D. P. *J. Am. Chem. Soc.* **2008**, *130*, 5459–5471.
(55) Lange, A.; Giller, K.; Hornig, S.; Martin-Eauclaire, M. F.; Pongs, O.; Becker, S.; Baldus, M. *Nature* **2006**, *440*, 959–962.
(56) Cady, S. D.; Schmidt-Rohr, K.; Wang, J.; Soto, C. S.; DeGrado, W. F.; Hong, M. *Nature* **2010**, *463*, 689–U127.
(57) Hu, F. H.; Luo, W. B.; Hong, M. *Science* **2010**, *330*, 505–508.
(58) Sharma, M.; Yi, M. G.; Dong, H.; Qin, H. J.; Peterson, E.; Busath, D. D.; Zhou, H. X.; Cross, T. A. *Science* **2010**, *330*, 509–512.
(59) Griffin, R. G. *Nat. Struct. Biol.* **1998**, *5*, 508–512.
(60) Opella, S. J. *Nat. Struct. Biol.* **1997**, *4*, 845–848.
(61) McDermott, A. E. *Curr. Opin. Struct. Biol.* **2004**, *14*, 554–561.
(62) Baldus, M. *Curr. Opin. Struct. Biol.* **2006**, *16*, 618–623.
(63) Gehman, J. D.; O'Brien, C. C.; Shabanpoor, F.; Wade, J. D.; Separovic, F. *Eur. Biophys. J. Biophys. Lett.* **2008**, *37*, 333–344.
(64) Bertini, I.; Emsley, L.; Lelli, M.; Luchinat, C.; Mao, J. F.; Pintacuda, G. *J. Am. Chem. Soc.* **2010**, *132*, 5558.
(65) Jovanovic, T.; McDermott, A. E. *J. Am. Chem. Soc.* **2005**, *127*, 13816–13821.
(66) Wickramasinghe, N. P.; Shaibat, M. A.; Ishii, Y. *J. Phys. Chem. B* **2007**, *111*, 9693–9696.
(67) Nadaud, P. S.; Helmus, J. J.; Kall, S. L.; Jaroniec, C. P. *J. Am. Chem. Soc.* **2009**, *131*, 8108–8120.
(68) Miller, Y.; Ma, B. Y.; Nussinov, R. *Proc. Natl. Acad. Sci. U.S.A.* **2010**, *107*, 9490–9495.
(69) Smith, D. P.; Smith, D. G.; Curtain, C. C.; Boas, J. F.; Pilbrow, J. R.; Ciccotosto, G. D.; Lau, T. L.; Tew, D. J.; Perez, K.; Wade, J. D.; Bush, A. I.; Drew, S. C.; Separovic, F.; Masters, C. L.; Cappai, R.; Barnham, K. J. *J. Biol. Chem.* **2006**, *281*, 15145–15154.
(70) Petkova, A. T.; Leapman, R. D.; Guo, Z. H.; Yau, W. M.; Mattson, M. P.; Tycko, R. *Science* **2005**, *307*, 262–265.
(71) Matsuba, Y.; Takahash., Y *Anal. Biochem.* **1970**, *36*, 182.
(72) Varadarajan, S.; Kanski, J.; Aksenova, M.; Lauderback, C.; Butterfield, D. A. *J. Am. Chem. Soc.* **2001**, *123*, 5625–5631.
(73) Schoneich, C.; Pogocki, D.; Hug, G. L.; Bobrowski, K. *J. Am. Chem. Soc.* **2003**, *125*, 13700–13713.
(74) Barnham, K. J.; Ciccotosto, G. D.; Tickler, A. K.; Ali, F. E.; Smith, D. G.; Williamson, N. A.; Lam, Y. H.; Carrington, D.; Tew, D.; Kocak, G.; Volitakis, I.; Separovic, F.; Barrow, C. J.; Wade, J. D.; Masters, C. L.; Cherny, R. A.; Curtain, C. C.; Bush, A. I.; Cappai, R. *J. Biol. Chem.* **2003**, *278*, 42959–42965.
(75) Tickler, A. K.; Smith, D. G.; Ciccotosto, G. D.; Tew, D. J.; Curtain, C. C.; Carrington, D.; Masters, C. L.; Bush, A. I.; Cherny, R. A.; Cappai, R.; Wade, J. D.; Barnham, K. J. *J. Biol. Chem.* **2005**, *280*, 13355–13363.
(76) Petkova, A.; Ishii, Y.; Balbach, J. J.; Antzutkin, O. N.; Leapman, R. D.; Delaglio, F.; Tycko, R. *Proc. Natl. Acad. Sci. U.S.A.* **2002**, *99*, 16742–16747.
(77) Petkova, A. T.; Yau, W. M.; Tycko, R. *Biochemistry* **2006**, *45*, 498–512.
(78) Pang, Y. P. *J. Mol. Model.* **1999**, *5*, 196–202.
(79) Branco, R. J. F.; Fernandes, P. A.; Ramos, M. J. *J. Phys. Chem. B* **2006**, *110*, 16754–16762.
(80) Peters, M. B.; Yang, Y.; Wang, B.; Fusti-Molnar, L.; Weaver, M. N.; Merz, K. M. *J. Chem. Theory Comput.* **2010**, *6*, 2935–2947.
(81) Ishii, Y.; Chimon, S.; Wickramasinghe, N. P. *J. Am. Chem. Soc.* **2003**, *125*, 3438–3439.
(82) Wickramasinghe, N. P.; Shaibat, M.; Ishii, Y. *J. Am. Chem. Soc.* **2005**, *127*, 5796–5797.
(83) Shaibat, M. A.; Casabianca, L. B.; Wickramasinghe, N. P.; Guggenheim, S.; de Dios, A. C.; Ishii, Y. *J. Am. Chem. Soc.* **2007**, *129*, 10968.
(84) Kervern, G.; Pintacuda, G.; Zhang, Y.; Oldfield, E.; Roukoss, C.; Kuntz, E.; Herdtweck, E.; Basset, J. M.; Cadars, S.; Lesage, A.; Coperet, C.; Emsley, L. *J. Am. Chem. Soc.* **2006**, *128*, 13545–13552.
(85) Miller, Y.; Ma, B.; Nussinov, R. *Chem. Rev.* **2010**, *110*, 4820–4838.
(86) Fields, C. A.; Fields, G. B.; Noble, R. L.; Cross, T. A. *Int. J. Peptide Protein Res.* **1989**, *33*, 298–303.
(87) Ishii, Y. *J. Chem. Phys.* **2001**, *114*, 8473–8483.
(88) Delaglio, F.; Grzesiek, S.; Vuister, G. W.; Zhu, G.; Pfeifer, J.; Bax, A. *J. Biomol. NMR* **1995**, *6*, 277–293.
(89) Kotecha, M.; Wickramasinghe, N. P.; Ishii, Y. *Magn. Reson. Chem.* **2007**, *45*, S221–230.
(90) Case, D. A. D.; Cheatham, I. T. E.; Simmerling, C. L.; Wang, J.; Duke, R. E.; Luo, R.; Merz, K. M.; Wang, B.; Pearlman, D. A.; Crowley, M.; Brozell, S.; Tsui, V.; Gohlke, H.; Mongan, J.; Hornak, V.; Cui, G.; Beroza, P.; Schafmeister, C.; Caldwell, J. W.; Ross, W. S.; Kollman, P. A. AMBER 8; University of California, San Fransisco, 2004.
(91) Hornak, V.; Abel, R.; Okur, A.; Strockbine, B.; Roitberg, A.; Simmerling, C. *Proteins-Struct. Funct. Bioinf.* **2006**, *65*, 712–725.
(92) Tsui, V.; Case, D. A. *J. Am. Chem. Soc.* **2000**, *122*, 2489–2498.
(93) Perez-Alvarado, G. C.; Martinez-Yamout, M.; Allen, M. M.; Grosschedl, R.; Dyson, H. J.; Wright, P. E. *Biochemistry* **2003**, *42*, 7348–7357.
(94) Strange, R. W.; Antonyuk, S. V.; Hough, M. A.; Doucette, P. A.; Valentine, J. S.; Hasnain, S. S. *J. Mol. Biol.* **2006**, *356*, 1152–1162.
(95) Koradi, R.; Billeter, M.; Wuthrich, K. *J. Mol. Graph.* **1996**, *14*, 51.
(96) Ryckaert, J. P.; Ciccotti, G.; Berendsen, H. J. C. *J. Comput. Phys.* **1977**, *23*, 327–341.
(97) Kale, L.; Skeel, R.; Bhandarkar, M.; Brunner, R.; Gursoy, A.; Krawetz, N.; Phillips, J.; Shinozaki, A.; Varadarajan, K.; Schulten, K. *J. Comput. Phys.* **1999**, *151*, 283–312.
(98) Brooks, B. R.; Bruccoleri, R. E.; Olafson, B. D.; States, D. J.; Swaminathan, S.; Karplus, M. *J. Comput. Chem.* **1983**, *4*, 187–217.

(99) Martyna, G. J.; Tobias, D. J.; Klein, M. L. *J. Chem. Phys.* **1994**, *101*, 4177–4189.
(100) Feller, S. E.; Zhang, Y. H.; Pastor, R. W.; Brooks, B. R. *J. Chem. Phys.* **1995**, *103*, 4613–4621.
(101) Deng, N. J.; Yan, L.; Singh, D.; Cieplak, P. *Biophys. J.* **2006**, *90*, 3865–3879.
(102) Zirah, S.; Kozin, S. A.; Mazur, A. K.; Blond, A.; Cheminant, M.; Segalas-Milazzo, I.; Debey, P.; Rebuffat, S. *J. Biol. Chem.* **2006**, *281*, 2151–2161.
(103) Lee, M. S.; Salsbury, F. R.; Brooks, C. L. *J. Chem. Phys.* **2002**, *116*, 10606–10614.
(104) Lee, M. S.; Feig, M.; Salsbury, F. R.; Brooks, C. L. *J. Comput. Chem.* **2003**, *24*, 1348–1356.